remote sensing

MDPI

Article

Flood Monitoring in Rural Areas of the Pearl River Basin (China) Using Sentinel-1 SAR

Junliang Qiu [1], Bowen Cao [1], Edward Park [2], Xiankun Yang [1,3,*], Wenxin Zhang [1] and Paolo Tarolli [4]

[1] School of Geography and Remote Sensing, Guangzhou University, Guangzhou 510006, China; qiujunliang@e.gzhu.edu.cn (J.Q.); 2111901040@e.gzhu.edu.cn (B.C.); 2112001058@e.gzhu.edu.cn (W.Z.)
[2] National Institute of Education and Asian School of the Environment, Nanyang Technological University, Singapore 639798, Singapore; edward.park@nie.edu.sg
[3] Rural Non-Point Source Pollution Comprehensive Management Technology Center of Guangdong Province, Guangzhou University, Guangzhou 510006, China
[4] Department of Land, Environment, Agriculture and Forestry, University of Padova, Agripolis, viale dell'Università 16, 35020 Legnaro (PD), Italy; paolo.tarolli@unipd.it
* Correspondence: yangxk@gzhu.edu.cn

Abstract: Flood hazards result in enormous casualties and huge economic losses every year in the Pearl River Basin (PRB), China. It is, therefore, crucial to monitor floods in PRB for a better understanding of the flooding patterns and characteristics of the PRB. Previous studies, which utilized hydrological data were not successful in identifying flooding patterns in the rural and remote regions in PRB. Such regions are the key supplier of agricultural products and water resources for the entire PRB. Thus, an analysis of the impacts of floods could provide a useful tool to support mitigation strategies. Using 66 Sentinel-1 images, this study employed Otsu's method to investigate floods and explore flood patterns across the PRB from 2017 to 2020. The results indicated that floods are mainly located in the central West River Basin (WRB), middle reaches of the North River (NR) and middle reaches of the East River (ER). WRB is more prone to flood hazards. In 2017, 94.0% flood-impacted croplands were located in WRB; 95.0% of inundated croplands (~9480 hectares) were also in WRB. The most vulnerable areas to flooding are sections of the Yijiang, Luoqingjiang, Qianjiang, and Xunjiang tributaries and the lower reaches of Liujiang. Our results highlight the severity of flood hazards in a rural region of the PRB and emphasize the need for policy overhaul to enhance flood control in rural regions in the PRB to ensure food safety.

Keywords: flood hazards; Sentinel-1 images; Google Earth Engine; Pearl River Basin

Citation: Qiu, J.; Cao, B.; Park, E.; Zhang, W.; Yang, X.; Tarolli, P. Flood Monitoring in Rural Areas of the Pearl River Basin (China) Using Sentinel-1 SAR. *Remote Sens.* **2021**, *13*, 1384. https://doi.org/10.3390/rs13071384

Academic Editor: Karem Chokmani

Received: 7 March 2021
Accepted: 2 April 2021
Published: 3 April 2021

1. Introduction

Numerous studies have shown that global warming may intensify the risk of flood hazards [1–3], especially in flood-prone regions [4]. Flood hazards can cause enormous damage to human society and the environment. During the period 1970–2015, a total of around 12,000 hydrologic disasters were reported globally, killing more than 3,530,000 people, disturbing more than 6.7 billion, and leading to total damage of more than US$ 2600 billion. For example, the 1998 floods in China caused an average economic loss of US$832.45 per family in the Hunan province of China [5]. In 2005, a catastrophic flood triggered by Hurricane Katrina caused hundreds of fatalities in New Orleans [6]. As the most common natural disaster [7–13], flood hazards cause enormous damage to the world every year. Thus, it is necessary to develop improved monitoring, mitigation, prevention, and assessment for flood hazards.

Flood monitoring is the precondition for flood mitigation and flood prevention, especially for large river basins like the Pearl River Basin (PRB), a prosperous and densely populated region with a total area of about 440,000 km^2 where flood locations and flood

extents are widely distributed. Without comprehensive and global observation of flood hazards, it is difficult to accurately implement flood mitigation and prevention measures, such as constructing reservoirs or embankments and promoting afforestation to prevent floods. This is especially true for floods in the PRB, China's second-largest river basin in terms of water discharge, with a highly developed economy, a large population, and several megacities, such as Shenzhen, Guangzhou, Hong Kong, and Macau. This combination of factors provided the motivation for this study. Floods often cause disastrous impacts on society, urban infrastructure, water resources, and agricultural activities. This is the case for all of China, where floods tend to have more dramatic impacts on agriculture than droughts [14].

Previous studies [14–19] on flood monitoring in PRB mainly employed gauging data from hydrological stations, focusing on the water level and flow during the flood peaks; few quantified the areal extent of flooding. However, such studies, only utilizing gauging data, were not successful in identifying flooding patterns in the rural and remote regions in PRB. This is because the number of hydrological stations is too sparse to reliably infer changes in water levels in rural and remote areas. Thus, most of the studies [20–27] just focused on the delta regions. The floods in the vast rural middle and upper reaches are still not well investigated. However, such regions are the key supplier of agricultural products and water resources for the entire basin, which creates a need for further study to explore floods in the entire basin. To implement a study covering the vast river basin, flood monitoring methods based on satellite images should be developed. Such techniques would add value by quantifying the area affected by flood hazards.

The development of remote sensing has allowed satellite imagery to be used for flood monitoring [28–36]. The PRB, mainly located in the subtropical zone, often is covered by clouds during the monsoon season. Thus, the regions affected by floods are often covered with clouds during the inundation period, making it extremely difficult to measure floods at the peak time using optical images (e.g., MODIS, Landsat, and Sentinel-2, etc.). Synthetic aperture radar (SAR) imaging can detect water bodies regardless of weather conditions. The Sentinel-1 SAR sensor, with a spatial resolution of 10 m and a swath up to 400 km, has the advantage of free access and short revisit times (~12 days in PRB), which is appropriate for monitoring floods in PRB. In this study, we investigated floods in the entire PRB based on Sentinel-1 is to find the trends of floods across the PRB, emphasizing the vast rural upper and middle reaches. Investigating the inundated croplands in such reaches is also important for the assessment of agricultural losses and the development of flood control measures in the PRB.

Thus, the aims of this study are to (i) propose a practical method to monitor floods in the cloudy PRB by integrating Sentinel-1 SAR images and observations at hydrological stations, (ii) identify flood patterns in the vast rural upper and middle reaches, and (iii) analyze the impacts of floods on croplands to emphasize the need for policy overhaul to enhance flood control in rural regions in the PRB to ensure food safety.

2. Materials and Methods

2.1. Study Area

The PRB, located in southern China, with an extent from 21°31′N to 26°49′N and 102°14′E to 115°53′E, (Figure 1), is controlled by subtropical monsoons with an annual average temperature from 14 to 22 °C and average precipitation from 1200 to 2200 mm. The total area of the PRB is about 440,000 km^2. It has an annual river runoff of 569.7 billion m^3. Basin-scale floods in PRB are primarily triggered by hydrometeorological extremes from May to July. PRB consists of the West River Basin (WRB), North River Basin (NRB) and East River Basin (ERB) (Figure 1). In the WRB, elevation decreases to the east from the Yunnan-Guizhou Plateau in western WRB. In the NRB and ERB, elevation decreases from north to south. Southeast PRB is the Pearl River Delta (PRD), consisting of several large metropolises, such as Guangzhou, Shenzhen, Hong Kong, and Macao.

Although precipitation is abundant in the basin, its spatial and temporal distribution is extremely uneven [37,38], which increases the risk of floods. Due to the rugged morphology and the densely distributed tributaries in the upper and middle reaches [39], water flows into the mainstream in a short period, resulting in floods with a high peak discharge [16]. This process consistently results in a large number of casualties and significant economic losses in PRB. Therefore, to prevent or mitigate flood hazards in the PRB, it is of great importance to investigate the characteristics of flooding patterns in the entire basin.

Since the PRB is the second largest basin in China and the PRD is one of the most prosperous regions in China, many studies have examined its flood hazards. Relevant studies on the flood-water level in the PRB showed that trends of the extreme water-level were decreasing in the upper part of PRD from 1951 to 2005 while increasing in the middle and lower part of PRD from 1951 to 2005 [15]; trends of the peak stream-flow were increasing in WRB and NRB from 1951 to 2010 while decreasing in ERB from 1951 to 2010 [17,18]. Relevant studies on flood frequency in the PRB showed a significantly increasing trend in flood events since 1980 [16]; losses caused by floods were also increasing before the 1990s while decreasing after the 1990s [40]; WRB and NRB were more prone to basin-scale flood hazards than ERB [14]. However, the time-series utilized in the aforementioned studies all ended before 2010. This study uses Sentinel-1 images from 2017–2020 to monitor floods in PRB. One of our key objectives was to improve flood monitoring methods for the PRB by combining Sentinel-1 images with hydrological data. We sought to update the recent flood trends in the entire PRB.

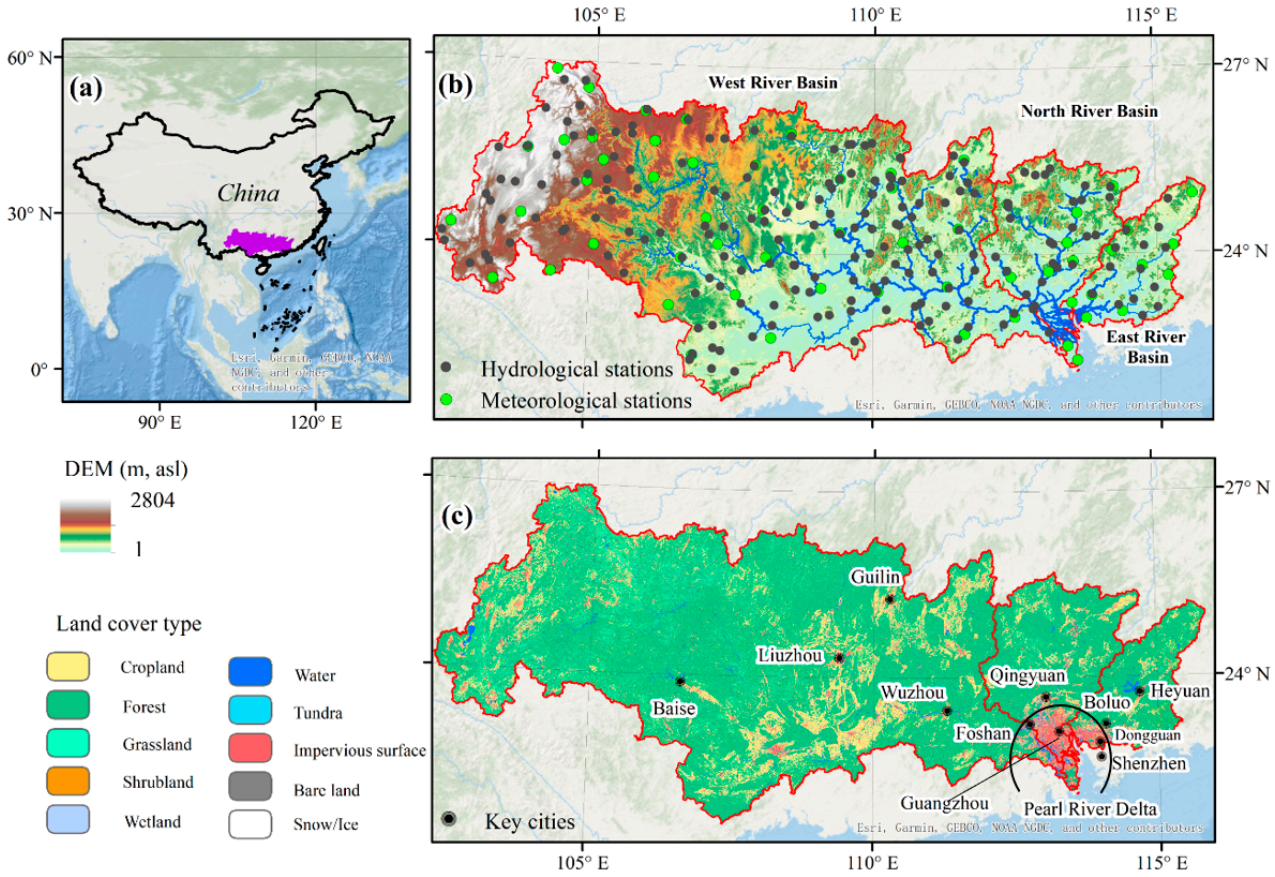

Figure 1. (**a**) Location of the Pearl River Basin (PRB) in China; (**b**) the distribution of meteorological stations and hydrological stations; (**c**) key cities in PRB and the land cover in PRB (circled region represents the Pearl River Delta).

2.2. Data Source

Sentinel-1 images are the data source for flood monitoring in this study. Sentinel-1 SAR ground range detected (GRD) products were acquired and analyzed in Google Earth Engine (GEE) platform (https://developers.google.com/earth-engine/datasets/catalog/COPERNICUS_S1_GRD, accessed on 22 Januray 2021), in which the Sentinel-1 images were preprocessed by removing thermal noise and underwent radiometric calibration and terrain correction. The VV polarization channel was used in this study, as this polarization has a good performance in open-water monitoring [41,42].

To select Sentinel-1 images for flood events in PRB, we first obtained specific time frames of basin-scale flood events from the national annual hydrological report (NAHP) provided by the Ministry of Water Resources of the People's Republic of China (MWR) (http://www.mwr.gov.cn/, accessed on 22 Januray 2021). According to the definition from MWR, when the water level of the Wuzhou Hydrological Station (Figure 1) reaches 18.5 m, it is considered as a basin-scale flood event in WRB; when the water discharges of Shijiao Hydrological Station in Qingyuan (Figure 1) and Boluo Hydrological Station (Figure 1) reach 12,000 m^3/s and 7000 m^3/s, it is considered as a basin-scale flood event in NRB and ERB, respectively. Since the Sentinel-1 images were available since February 2015, we checked the reports from 2015 to 2019 to confirm the flooding periods in WRB, NRB and ERB and searched Sentinel-1 SAR images acquired from 2015 to 2020 in GEE and the corresponding near-real-time (NRT) Sentinel-1 images. We then corresponded the NRT Sentinel-1 images with basin-scale flood events in PRB for 2017, 2019 and 2020. Collectively, we selected 66 scenes of Sentinel-1 images, half of which were during an inundation period and the rest outside of any inundation period. The optical imagery of Sentinel-2, with a spatial resolution of 10 m, is appropriate to validate the water body monitoring results based on Sentinel-1 SAR imagery under cloud-free conditions. Each footprint of the Sentinel-1 image used in the study can be seen in Figure 2, and Table 1 shows the corresponding sensing date of Sentinel-1 images. We did not add the footprints of the Sentinel-1 images in some regions of western PRB because there are almost no floods monitored by Sentinel-1 SAR images in this region. A scene of cloud-free Sentinel-2 image was used for accurate assessment of the water body extraction based on the Sentinel-1 image.

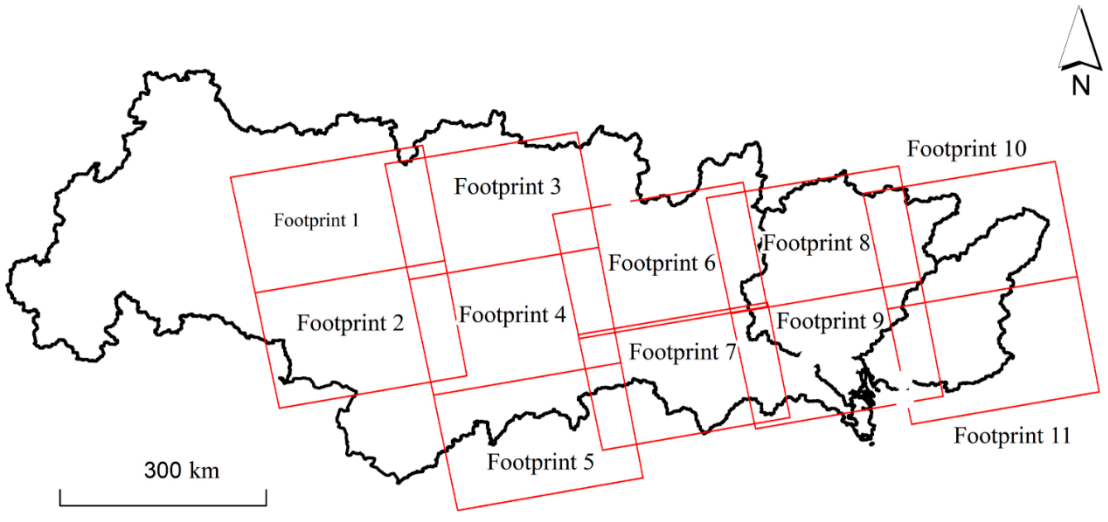

Figure 2. Locations of footprints of Sentinel-1 images.

Table 1. Sensing dates of Sentinel-1 images in different footprints in Figure 2 (before and during floods).

Footprint	2017		2019		2020	
	Before	During	Before	During	Before	During
1	7 June	13 July	28 May	15 July	22 May	3 June
2	7 June	13 July	28 May	15 July	22 May	3 June
3	21 May	8 July	16 June	22 July	5 May	10 June
4	21 May	8 July	11 May	22 July	5 May	10 June
5	21 May	8 July	11 May	22 July	5 May	10 June
6	9 June	3 July	30 May	17 July	12 May	5 June
7	9 June	3 July	30 May	17 July	12 May	5 June
8	4 June	10 July	14 March	19 April	7 May	12 June
9	4 June	10 July	14 March	19 April	7 May	12 June
10	6 May	5 July	8 May	13 June	2 May	7 June
11	6 May	5 July	8 May	13 June	2 May	7 June

Daily precipitation data, collected from China Meteorological Data Network (CMDN) (http://www.data.cma.cn, accessed on 22 Januray 2021), was used to support the analysis of flooding patterns. The distribution of meteorological stations in the PRB is shown in Figure 1. The ERA5 Daily aggregates products (https://developers.google.com/earth-engine/datasets/catalog/ECMWF_ERA5_DAILY, accessed on 22 Januray 2021), which are the latest climate reanalysis datasets produced by the European Centre for Medium-Range Weather Forecasts (ECMWF), were also used in this study. The products include climate indices, such as daily air temperature, daily precipitation, daily surface pressure, etc. We combined the total precipitation of ERA5 with daily precipitation from CMDN to analyze the rainfall patterns during the flood periods.

To assess the agricultural losses caused by flood hazards in the rural middle and upper reaches, a set of 10 m resolution global land cover maps (Figure 1) [43] derived from Sentinel-2 images was used to calculate the inundation area of cropland.

To verify the flood monitoring results derived from Sentinel-1 images, we also obtained the daily water level records of 199 hydrological stations during the flood period in 2017 from the Hydrological Statistics Year Book of China. The dataset included the water level and flow recorded at 8:00 and 14:00. In this study, we chose the higher value of the water levels as the daily highest water level. The distribution of hydrological stations is shown in Figure 1.

In addition, we employed some supplementary data released in 2012 by the Pearl River Water Resources Commission (PRWRC), which consists of flood-prone areas delineated by the PRWRC and the spatial distribution of embankments. We compared the flood areas in this study with the flood-prone areas outlined by PRWRC and the spatial distribution of embankments to understand embankments' role in flood mitigation.

2.3. Flood Monitoring Using Sentinel-1 Images

In this study, a dynamic threshold method (Otsu's method), which aims to maximize between-class variability [44], was used to detect water bodies in satellite images [42,45–48]. A single threshold way for SAR images to distinguish water body and non-water body could cause bias. Different incident angles, aerosol concentrations, and other various conditions, backscatter of SAR images in different times or orbits would have different distributions. This method performs well when an image has a bimodal distribution, and the object area occupies more than 30% of the whole image [49]. Figure 3 shows the flowchart summarizing the steps of flood monitoring. However, Sentinel-1 images in the PRB generally do not have bimodal distributions, and the water body area is much less than 30% of the whole image. Thus, we first selected a region containing enough open water pixels with a histogram with a bimodal distribution. Usually, we choose the area

around the largest lake in each Sentinel-1 SAR image to maximize the sample for Otsu's method. As shown in Figure 4, region (b) was selected, and it had a bimodal distribution. The Otsu's method would perform well with images like this one. We then performed the dynamic threshold method with the region to derive a threshold value, which will then be used to binarize each selected Sentinel-1 image. Finally, we checked the water body monitoring results in some regions where the water body shapes are more complicated, such as the region (c) in Figure 4. If the water body monitoring results are close to the original Sentinel-1 SAR images, the threshold value can be used for further processing. The above steps were all performed on the GEE platform. The results were then saved and exported to the local device. Due to the rugged morphology in the upper PRB, the shadows would reduce the accuracy of water body detection. Usually, elevation and slope derived from the digital elevation model (DEM) were used to remove the shadows [50]. However, the shadows could not be completely removed. Here, we converted the raster results into vector data and visually removed shadows within ArcGIS Desktop. To investigate the spatial patterns of floods, we identified the flooded regions based on the rule: if the water body exceeded the river channel or occupied other land covers, the location would be marked as a flood location.

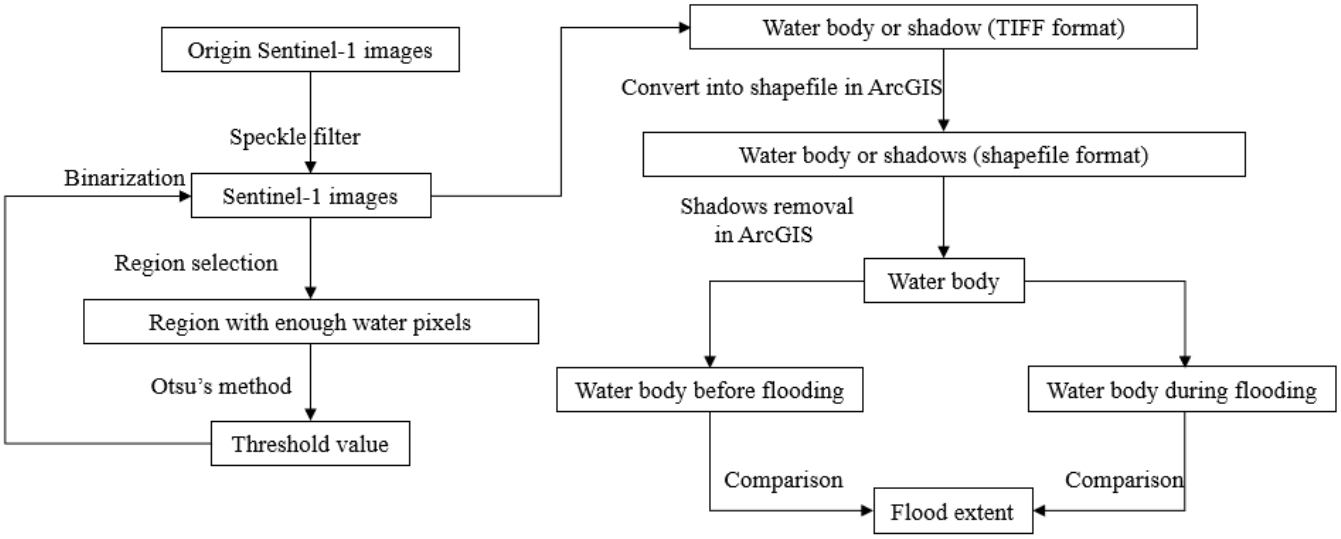

Figure 3. Flowchart of flood monitoring based on Sentinel-1 images.

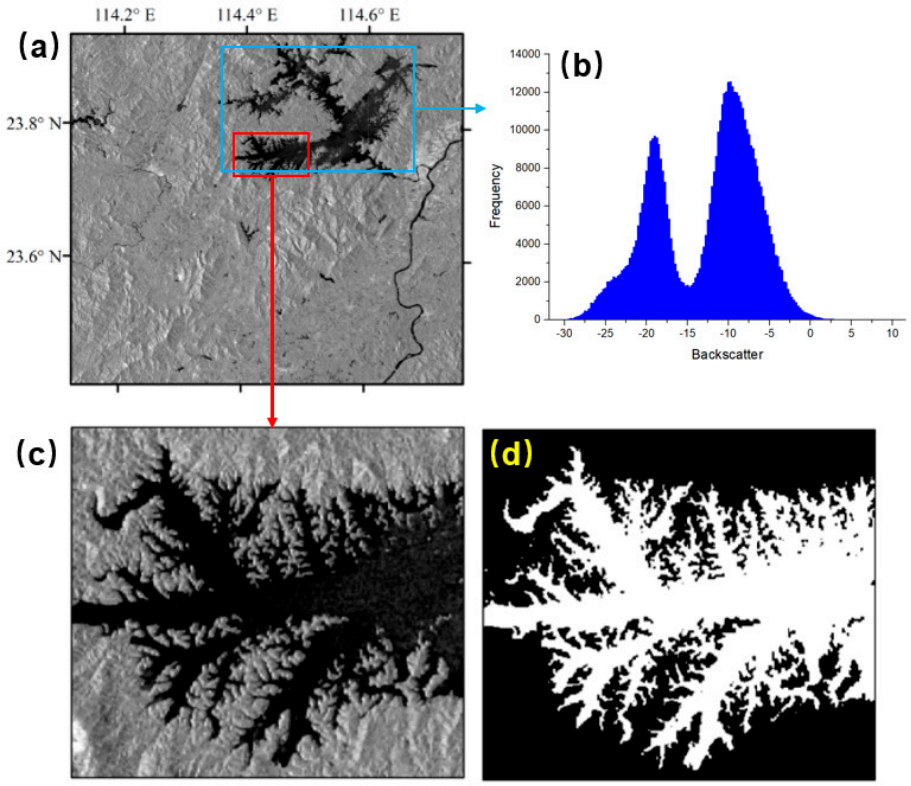

Figure 4. Selection of an appropriate region to derive the threshold for processing Sentinel-1. (a) Orignal Sentinel-1 image on 29/10/2020; (b) Histogram of backscatter distribution in the region contained by blue box in (a); (c) Region contained by red box in (a); (d) Water body extraction based on Sentinel-1 image and Otsu's method.

2.4. Corresponding Validation for Water Body Extraction Based on Sentinel-1 Images

With a spatial resolution of 10 m (Table 2), Sentinel-2 images are useful for assessing the water body extraction. A cloud-free Sentinel-2 image obtained on 26 October 2020 was selected to extract water body using a support vector machine classifier, compared with the corresponding result obtained from Sentinel-1 image on 29 October 2020. The delineation results derived from Sentinel-1 and Sentinel-2 images are quite consistent (Figure 5), and the overall accuracy using kappa's coefficient was 96.1%. In the region contained by the red box (Figure 5c,d), the Sentinel-2 image performs somewhat better than the Sentinel-1 SAR image in monitoring small water bodies, such as the narrow lakes. However, the shapes of the typical floods in PRB are usually wide enough to be monitored by Sentinel-1 SAR images.

Table 2. Band information for Sentinel-2 and Sentinel-1 images.

Sensor	Band	Wavelength	Spatial Resolution (m)
Sentinel-2	Band2-Blue	492.4 nm	10
Sentinel-2	Band3-Green	559.8 nm	10
Sentinel-2	Band4-Green	664.6 nm	10
Sentinel-2	Band8-NIR	832.8 nm	10
Sentinel-1	C-band	5 cm	10

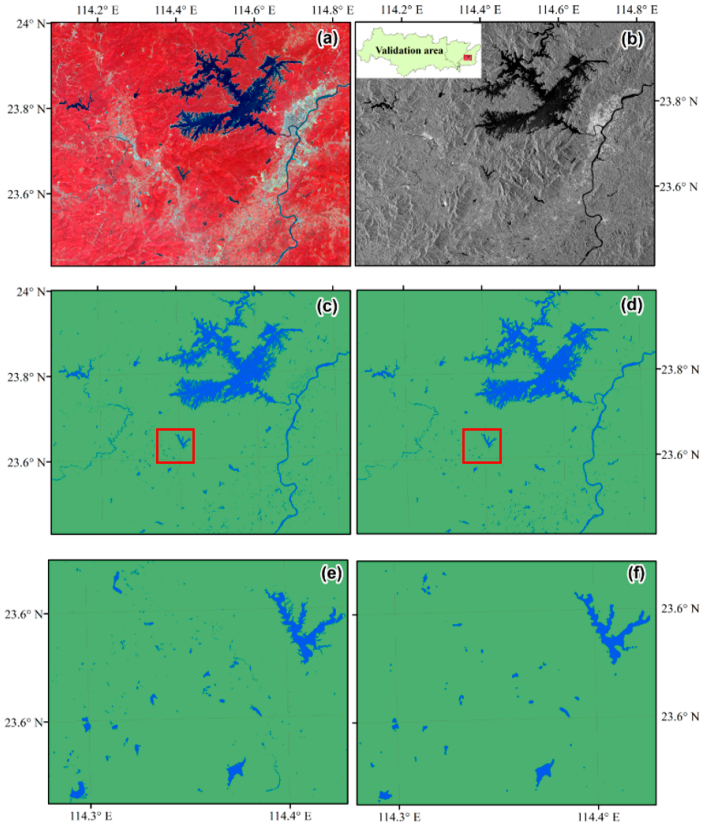

Figure 5. Assessment of the accuracy of the water body extraction based on Sentinel-1 images. (a) Sentinel-2 image (R: B8; G:B4; B:B2) on 26/10/2020; (b) Sentinel-1 image on 29/10/2020; (c) Water body extraction based on Sentinel-2 image; (d) Water body extraction based on Sentinel-1 image; (e) Region contained by the red box in (c); (f) Region contained by the red box in (d).

2.5. Interpolation for Precipitation Data

As shown in Figure 1, only 50 meteorological stations are available in the PRB, which is relatively sparse against the vast extent of the PRB. The spatial resolution of the daily total precipitation product from ERA5 is 0.25 arc degrees, which is relatively low. Thus, to improve the coverage of meteorological stations and the precipitation map's readability, we combined the precipitation data from CMDN with the daily total precipitation of ERA5 to generate a precipitation map (spatial resolution: 1 km) using the Kriging interpolation method. These precipitation maps were used in the analysis of flood patterns.

3. Results

3.1. Flooding Patterns in the PRB

According to the reports by NAHP of 2017, 2019 and 2020, basin-scale floods in the WRB happened only in 2017, 2019 and 2020. A basin-scale flood event in NRB happened only in 2020. In ERB, no basin-scale flood event happened in the study period. Table 1 presented the peak time and flood duration for each flood event. To make a comprehensive analysis of flood monitoring across the whole PRB, we used the measurement of the maximum accumulated precipitation for two consecutive weeks in 2017, 2019 and 2020 as the flood period because usually, the duration of floods in the PRB is about two weeks. We also derived the flood periods in the NRB or ERB. The obtained flood periods in WRB, NRB, and ERBare shown in Table 3.

Table 3. Flood peak time and corresponding flood period in West River Basin (WRB), North River Basin (NRB) and East River Basin (ERB).

Year	WRB		NRB		ERB	
	Peak	Period	Peak	Period	Peak	Period
2017	4 July	26 June–19 July	-	26 June–19 July	-	26 June–19 July
2019	10 July	1 July–14 July	-	12 April–26 April	-	4 June–18 June
2020	8 June	1–14 June	9 June	1–15 June	-	1–15 June

Collectively, flood locations were consistent with the spatial distribution of the precipitation during the flood events in 2017, 2019 and 2020 (Figure 6). Following Figure 1, flood locations are mainly distributed in flatlands along the rivers, especially in the middle reaches of the WRB. The western part of WRB is the rugged Yunnan-Guizhou Plateau, where the steep terrain makes it difficult to form typical floods that can be identified by Sentinel-1 images, although some of the regions experienced intense rainstorms. Similarly, in the northern part of NRB, no floods were observed, probably due to the rugged terrain. In the delta area, the most populated region in the PRB, no floods were observed, probably due to the dike construction that mitigated flood expansion.

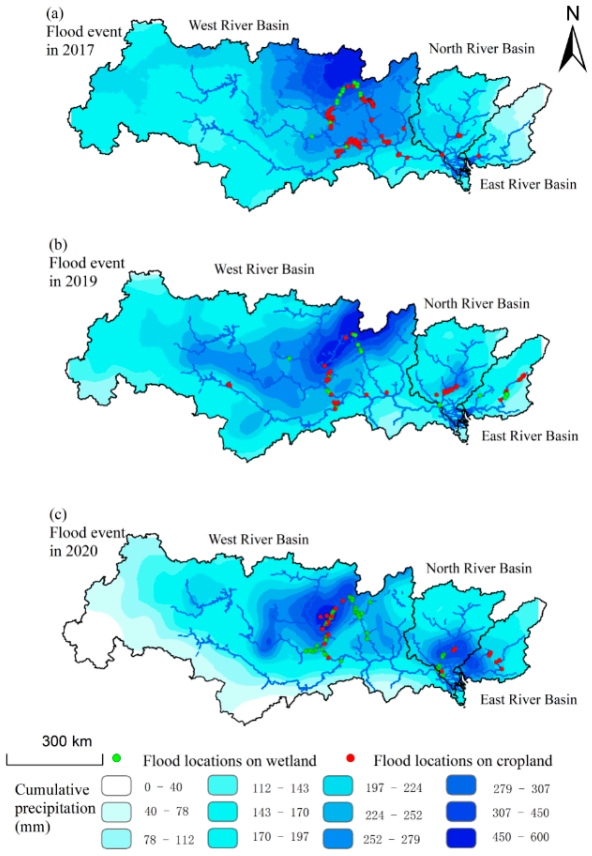

Figure 6. (a) Flood event in 2017 in PRB; (b) Flood event in 2019 in PRB; (c) Flood event in 2020 in PRB. Corresponding flood periods are shown in Table 3.

As shown in Figure 5, flood locations in the PRB are primarily located in WRB. In 2020, given the same magnitude of rainstorms with cumulative precipitations of more than 450 mm, flood locations in the WRB were more numerous than the combined flood locations of NRB and ERB. Some sites and tributaries, where floods repeatedly occurred in 2017, 2019 and 2020, should be considered to mitigate and prevent flood hazards.

Table 4 presented the specific number of flood locations identified on wetlands and croplands in PRB. Regarding the number of flood locations and flood extents, floods in 2017 were more severe than those in 2019 and 2020. The number of flood locations on croplands in 2017 was 91, much higher than the other two years. In 2017, numerous flood locations were identified in southern WRB, but few were observed in 2019 and 2020.

Table 4. Number of flood locations identified from wetlands and croplands in 2017, 2019 and 2020.

Year	WRB		NRB		ERB		PRB	
	Wetland	Cropland	Wetland	Cropland	Wetland	Cropland	Wetland	Cropland
2017	29	84	6	6	0	1	35	91
2019	12	15	2	12	8	9	22	36
2020	41	18	5	3	0	5	46	26

3.2. Inundation Areas of Cropland and the Critical Flooding Regions

Table 5 shows the inundated croplands in the PRB, corresponding to the floods in 2017, 2019 and 2020. It should be noted that the inundation areas of cropland in Table 5 were slightly smaller than the actual inundation areas because the results were derived from NRT Sentinel-1 images. When assessing the losses caused by flood hazards, the inundation areas of cropland is a direct and important indicator that could be calculated using a 10 m resolution land cover map (Figure 1).

Table 5. Inundation areas of cropland in PRB (unit: hectare).

Year	WRB	NRB	ERB	Total
2017	9480	460	40	9980
2019	1840	950	320	3110
2020	2310	360	260	2930

The floods in 2017 were the most serious, especially in the WRB, with a total of 9980 hectares of inundated croplands. Flooded croplands in WRB were also much more extensive than in NRB or ERB. WRB should be prioritized for the implementation of flood prevention and mitigation measures for cropland protection. However, the severe losses caused by floods in NRB and ERB should not be ignored because hundreds of hectares of inundated cropland were also identified in the NRB and ERB. For example, in 2019, there were 950 hectares and 320 hectares of inundated cropland in the NRB and ERB, respectively. Regarding the impact on agriculture in the PRB and the number of flood locations in the PRB, we can conclude that WRB was exposed to the highest flood risk than NRB and ERB. The risk of flood in the NRB is slightly higher than in ERB.

In terms of flooding recurrence, some locations were flooded repeatedly in 2017, 2019, and 2020; Guilin is such an example, with a large amount of inundated cropland (Figure 6). As shown in Figure 7, the city is located in a narrow basin, surrounded by rugged mountains. This geomorphological condition is conducive for the accumulation of runoff during flood periods, leading to the rapid rise in water level in a short period. The location was often a rainstorm center during hydrometeorological extremes in 2017, 2019 and 2020, probably due to the interaction between monsoon and the terrain in PRB.

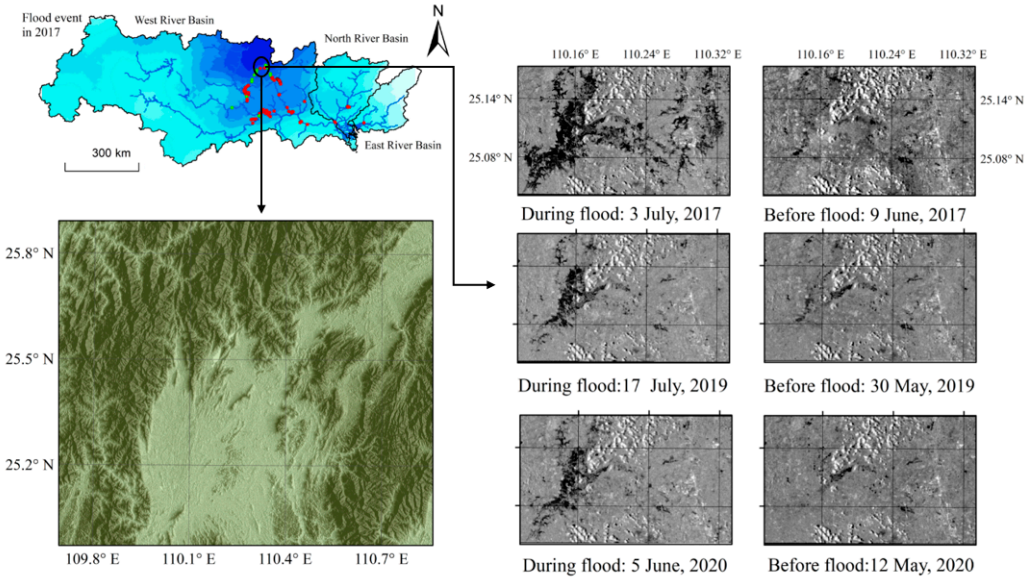

Figure 7. Locations are mainly affected by flooding in Guilin, Guangxi Province, China. Lower left panel is the integration between the DEM map and the hill shade map.

Apart from recurring flood areas, according to Figure 6, we can find that some river sections are exposed to higher flood risk, for example, the river sections of Yijiang, Luoqing, and Qian rivers (Figure 8). In addition, many flooded croplands could be found along the Lijiang and Xunjiang tributaries during the 2017 flood. Thus, the river sections of the Yijiang, Luoqingjiang, Qianjiang, Lijiang and Xunjiang rivers and the lower section of the Liujiang River are critical river sections with higher flood risk (Figure 8). In Table 6, we list the number of flood locations distributed along the critical river sections; during the 2017 flood, the corresponding proportion was 75.0%. It is apparent that flooded croplands are also mainly located along critical river sections, with 92.3% in 2017, 59.1% in 2019 and 78.7% in 2020, respectively. This analysis indicated that the regions along the major river sections have a higher flood risk in the WRB.

Table 6. Statistics for the number of flood locations and inundated croplands (unit: hectare) along critical river sections (CRS) and other river sections (ORS).

Year	Amount of Flood Locations			Inundation Areas of Cropland		
	CRS	ORS	Total	CRS	ORS	Total
2017	78 (75.0%)	26 (25.0%)	104	9267 (92.3%)	713 (7.7%)	9980
2019	20 (32.8%)	41 (67.2%)	61	1839 (59.1%)	1271 (40.9%)	3110
2020	46 (60.5%)	30 (39.5%)	76	2307 (78.7%)	623 (21.3%)	2930

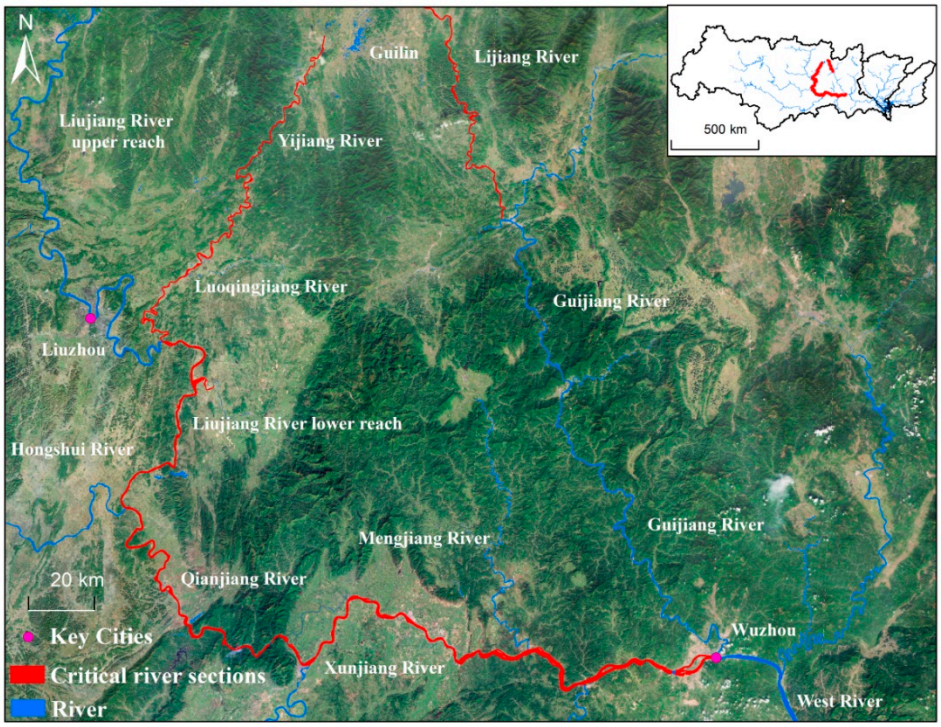

Figure 8. Critical river channels with higher flood risk.

4. Discussion

4.1. Uncertainty Analysis

Since the Sentinel-1 images used in this study were NRT SAR images, it is difficult to delineate flood extents at the flood peak time. Thus, the flood extents monitored in this study are inevitably smaller than the actual ones. For example, in the 2017 flood, the most critical flooding regions were covered by the footprints in Figure 9b, which showed that the sensing date (2017/7/3) was slightly later than the peak time (2017/7/2) at Guilin Hydrological Station (Figure 9c). Due to the limitation of the return period of Sentinel-1 images, if the sensing date was not in the period that the water level exceeded the warning water level, we had to select the NRT Sentinel-1 images. However, the flood monitoring results in this study still provided reliable flood locations and extent. For example, in Figure 9, the sensing date was very close to the date of flood peak at the Guilin Hydrological Station and was in the period that the water level exceeded the warning water level at Wuzhou hydrological station. Therefore, the flood extent monitored by the Sentinel-1 image in the footprints should be slightly smaller than the actual flood extent.

The spatial resolution of Sentinel-1 images in this study is 10 m, which means that it is difficult for Sentinel-1 images to monitor a flooded area of fewer than 100 m^2. In addition, no flood locations were found in the western WRB and northern NRB, likely owing to the steep channel in these rugged regions and relatively low precipitation. However, Sentinel-1 SAR imagery is valuable for monitoring floods because it can monitor extensive floods (more than 100 m^2) regardless of weather conditions.

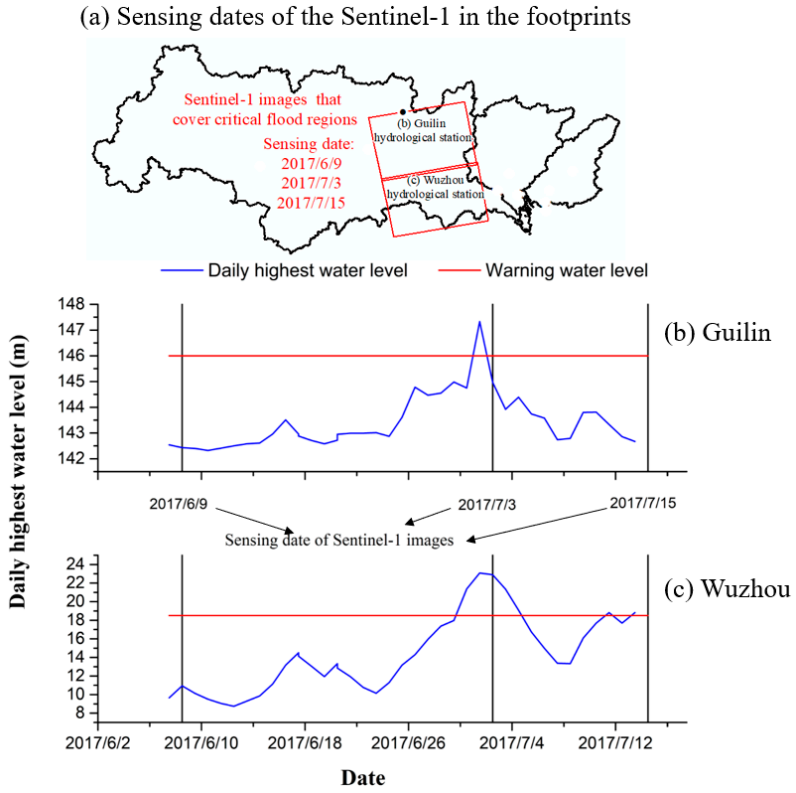

Figure 9. Comparison of the return period of Sentinel-1 images in major flooding regions corresponding to the date of flood peaks. (**a**) Sensing dates of the Sentinel-1 in the footprints; (**b**) daily highest water level at Guilin Hydrological Station; (**c**) daily highest water level at Wuzhou Hydrological Station.

4.2. Comparison of Flood Monitoring Results

To contrast the advantages and disadvantages of flood monitoring based on Sentinel-1 images and hydrological data, we compared the flood monitoring results derived from Sentinel-1 images and daily highest levels of 199 hydrological stations during the 2017 flood. There were 34 stations with water levels exceeding the warning water level in the range of 0.01 m to 5.33 m. The distribution of hydrological stations that exceeded the warning water level was consistent with the spatial distribution of flood locations derived from Sentinel-1 images.

As shown in Figure 10, although we used the hydrological data from 199 hydrological stations, much more than previous studies [14–17,37,40], some river sections were still not covered by hydrological stations. Therefore, flood monitoring results only based on hydrological data would undoubtedly cause deviation in such regions or river sections with sparse or without hydrological stations. Sentinel-1 images could be a reasonable alternative in such regions.

Although the Sentinel-1 images could cover the whole PRB, some flood locations have not been monitored by Sentinel-1 images yet. For example, at Rongshui, Zhaoping and Changan, the observed highest water levels are 5.27 m, 5.25 m and 4.01 m higher than their corresponding warning water levels, but failed to be identified by Sentinel-1 images. There were two probable reasons for this phenomenon. One reason could be that the hydrological stations were located in a very narrow valley, and Sentinel-1 images failed to monitor the water body due to its spatial resolution of 10 m. For instance, combining Figures 8 and 10, we can find that Zhaoping Hydrological Stations were located in a very narrow valley, which limits the Sentinel-1 SAR observation due to the terrain effects. Another reason could be the relatively low time resolution of Sentinel-1 images. As shown in Figure 11, at Rongshui Hydrological Station, the flood peak happened on 2 July 2017, with

5.27 m exceeding the warning water level. On 3 July 2017 (sensing date of Sentinel-1 image), the water level already dramatically dropped to 1.57 m below the warning water level. Regarding such a short flood period, it is challenging to identify flood extent around this station using Sentinel-1 images with a usual return period of 12 days.

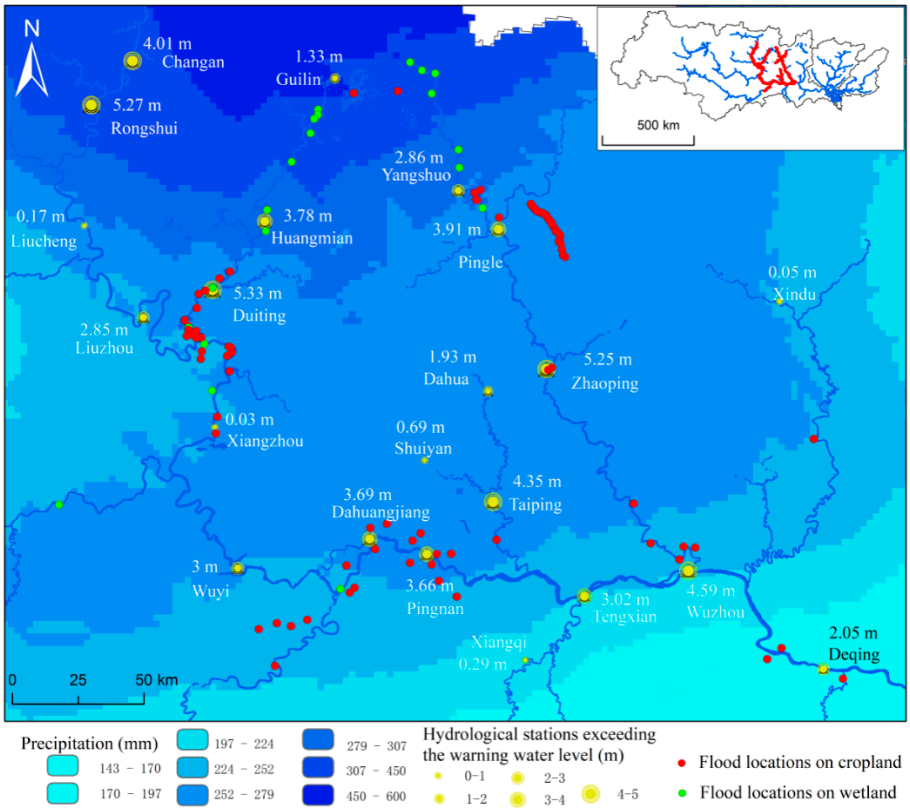

Figure 10. Flood monitoring results derived from Sentinel-1 images and hydrological data.

According to Figures 1 and 11, the duration of floods in the lower reaches and flatlands was significantly longer. For example, in the hydrological stations of Deqing, Wuzhou, Dahuangjiangkou, and Pingnan, periods that daily highest water exceeded waring water level were 3, 5, 6 and 6 days, respectively. Usually, the shortest return period of Sentinel-1 images is 12 days in the PRB. Thus, Sentinel-1 images could monitor a flood event within the expanding period of up to 6 days. Moreover, floods lasted for very short periods at Changan and Duiting, which were in the upper reaches of WRB; it was also difficult to monitor these floods with Sentinel-1 images. At Guilin station, which is also in the upper reach, the daily water level exceeded warning water levels for just one day, but, as shown in Figure 7, the region around Guilin station is a lowland surrounded by steep mountains. As such, flooding could be sustained for a longer period. Overall, it is more appropriate for Sentinel-1 images to monitor floods in flat regions.

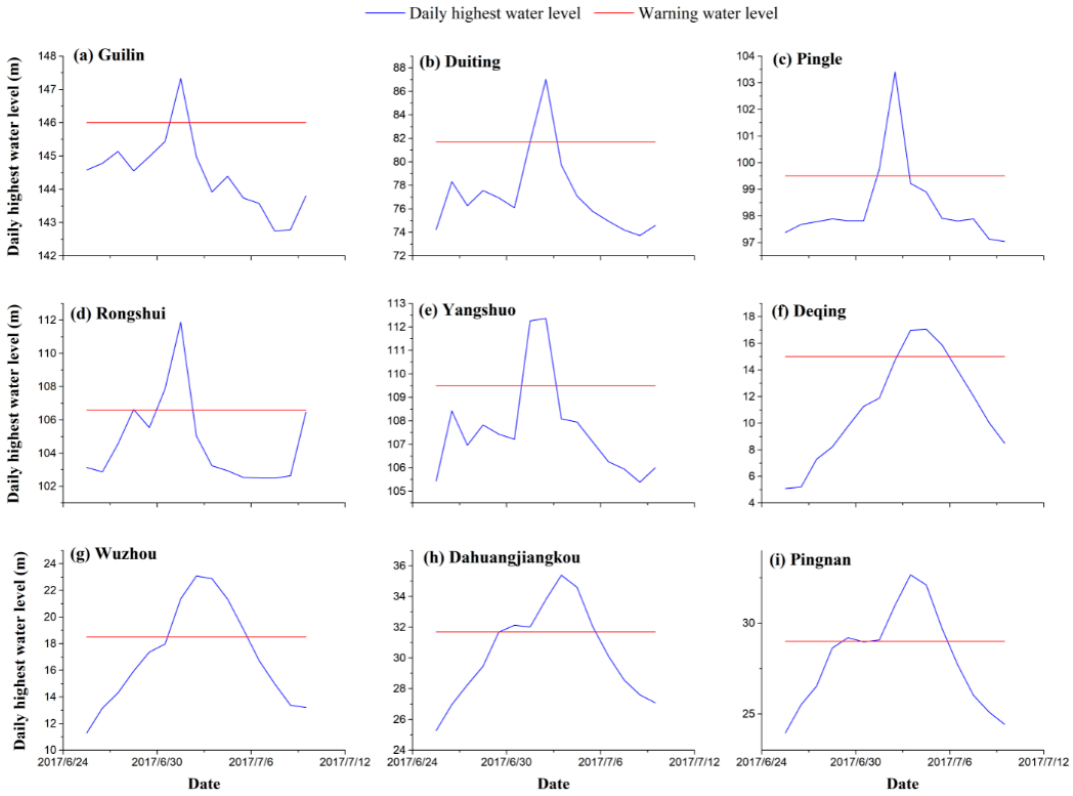

Figure 11. The daily highest water level at some key hydrological Stations during the 2017 flood. (**a**) Guilin Station; (**b**) Duiting Station; (**c**) Pingle Station; (**d**) Rongshui Station; (**e**) Yangshuo Station; (**f**) Deqing Station; (**g**) Wuzhou Station; (**h**) Dahuangjiangkou Station; (**i**) Pingnan Station.

In conclusion, compared with hydrological data in the scope of flood monitoring, Sentinel-1 images have the advantage of spatial continuity and the disadvantage of relatively low time resolution. Thus, it is recommended to combine radar images with hydrological data to monitor flood dynamics comprehensively.

4.3. Comparison with Previous Studies

Since this study time period was only three years, we were unable to examine long-term trends of flood hazards in the PRB, which was different from studies based on long-term hydrological data. However, flood monitoring results derived from Sentinel-1 images and long-term hydrological data are still comparable.

Regarding the scope of flood risk, this study showed that the WRB is under higher flood risk than the NRB and ERB. Zhang et al. [14] reported that annual peak flood flow increased significantly in the northeastern WRB (including central WRB mentioned above) and northern NRB during the period 1981–2010. Similarly, Gu et al. [18] reported that peak flood flow increased in WRB and NRB's mainstream during the period 1951–2010. Higher flood risk in WRB reported by Zhang and Gu is consistent with this study. However, this study showed no floods in the northern NRB, which was different from Zhang and Gu's results. As shown in Figure 1, northern NRB is a rugged region, where it is likely that no typical floods happened in 2017, 2019 and 2020. Also, rising peak flood discharge was not equivalent to the case that water overflows their banks. Different time series could also be the reason for the difference in study results. In the ERB, it was generally considered that flood peak was decreasing [17,18]. In this study, we did not observe any flood hazard trends in the ERB due to the short time series. However, according to the reports of NAHP in 2017, 2019 and 2020, no basin-scale flood event was reported, reflecting that ERB is indeed under relatively lower flood risk. Lu et al. [51] conclude that

rapid channel incision in the PRD due to sand mining and trapping of sediment by impoundments had caused water level decrease, which would reduce the flood risk. The construction of embankments and reservoirs would also significantly regulate river flow and decrease flood risk in the ERB.

NAHP is the official hydrological report released by the MWR. Descriptions about floods in the NAHP mainly included flood peak flow, flood peak water level, name of the river section and the return period of the corresponding flood events. According to the NAHP, in 2017, Luoqingjiang tributary suffered the second-largest flood after 1954; Lijiang tributary and Mengjiang tributary suffered a flood with a return period of 50 years. We could not evaluate the flood return period in PRB since the Sentinel-1 images were only available since 2015; however, according to the NAHP in 2017, floods in 2017 in the PRB were the most serious over the past two decades. According to Figure 6, we can infer that floods in 2017 were more severe than those in 2019 and 2020; this is consistent with the NAHP in 2017. However, the NAHP was generated based on hydrological data, lacking the information of flood extents and assessing the losses caused by floods. For instance, the NAHP in 2017 reported that the Lijiang tributary suffered a severe flood with a return period of 50 years. As shown in Figure 12, this flood event also affected the Rongjin River tributary. Water overflowed the banks along more than 40 km river section, with about 60 villages affected and about 496.2 hectares of croplands inundated. However, the NAHP in 2017 missed this extremely severe flood event around the Ronjin River. Without the monitoring results from remote sensing images, reports in NAHP would miss specific details of flood extents and inundated area of croplands. Thus, to make a more comprehensive annual hydrological report and provide a better reference for the public, we recommend MWR to improve NAHP by combining hydrological data and remote sensing images to monitor floods.

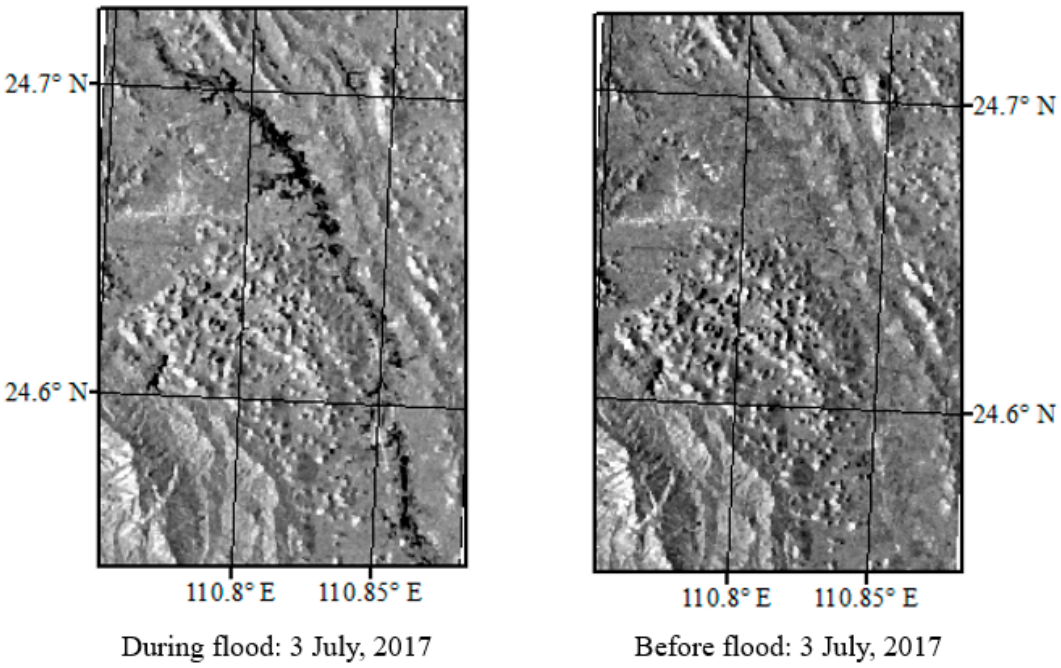

Figure 12. Flood event in 2017 along the Rongjin River and the original Sentinel-1 images.

For further validation of flood monitoring results based on Sentinel-1 images, we compared the flood locations in this study with the distribution of the regions prone to flood hazards obtained from the Comprehensive Atlas of the Pearl River Basin [52]. It

should be noted that the map was published in 2012, and the criteria for delimiting risk zones were based on the monitoring results of long-terms hydrological data before 2012.

In Figure 13, the flood locations in this study occurred in the regions prone to flood. However, some flood locations in this study were not identified as flood-prone areas by the map. For example, Figures 9 and 13 show that in the lower reaches of Luoqingjiang and Liujiang tributaries, many flood locations on croplands were not covered by the map. Figures 12 and 13 also show that flood locations along the Rongjin tributary were excluded from the map. The cases in the river sections of Luoqingjiang, Liujiang and Rongjin tributaries further illustrate that the map failed to identify the flooded areas with few hydrological stations available. Thus, we emphasize that it is imperative to combine remote sensing techniques and hydrological data to monitor floods.

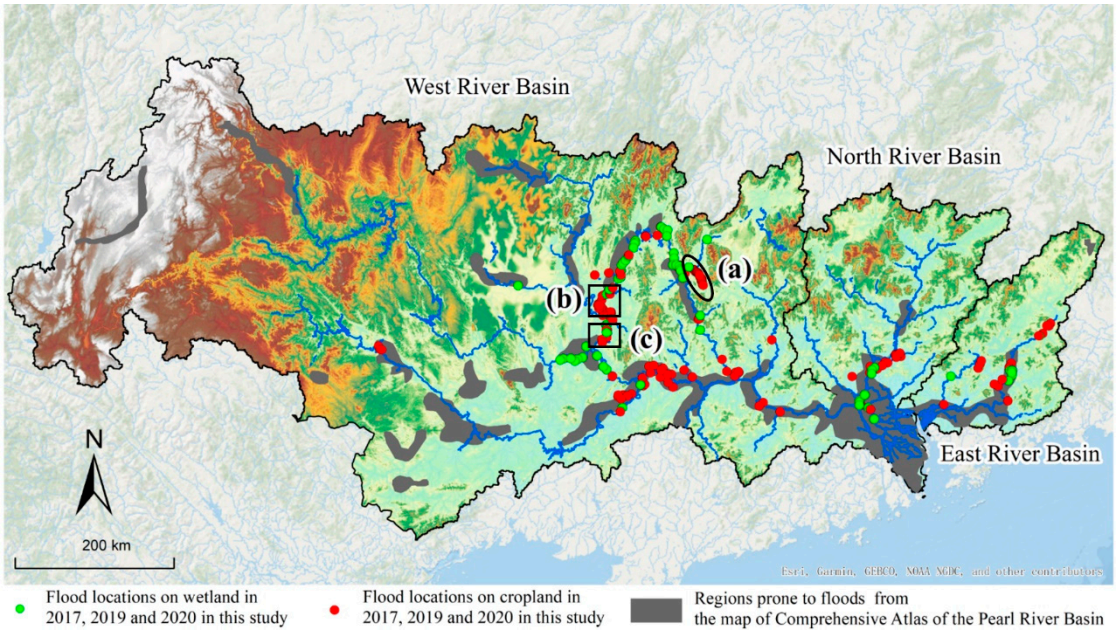

Figure 13. Comparison between the flood locations obtained in this study and the spatial distribution of sections prone to flood hazards from the map of Comprehensive Atlas of the Pearl River Basin published by PRWRC [52]. (**a**) Flood locations along Rongjin tributary; (**b**) flood locations along Liujiang tributaries; (**c**) flood lotions along Luoqingjiang tributaries.

Even though it was reported as a region prone to floods in Figure 13 in the western WRB, no floods were observed in the study period. In the PRD, some flood locations in the upper reaches in this study are consistent with the distribution of regions prone to floods. However, in the PRD, no flood locations were identified in this study, but they are denser regions prone to floods in the reported map (Figure 13). Sand mining and sediment impoundment by reservoirs had caused river channel incision. Lu et al. [51] reported that more than 40% of the river channels had down cut over 2 m between 1992 and 1999, and the deepest cut down was 9.86 m. The drastic incision of the river channels would cause a lower water level with the same river flow. Additionally, the construction of embankments would also mitigate flood hazards. As shown in Figure 14, the construction of embankments effectively mitigated the flood in PRD. In the upper reaches of the central WRB and upper reaches of ERB, few embankments were built. Figure 14 thus summarized the effects of embankments on flood mitigation in PRB.

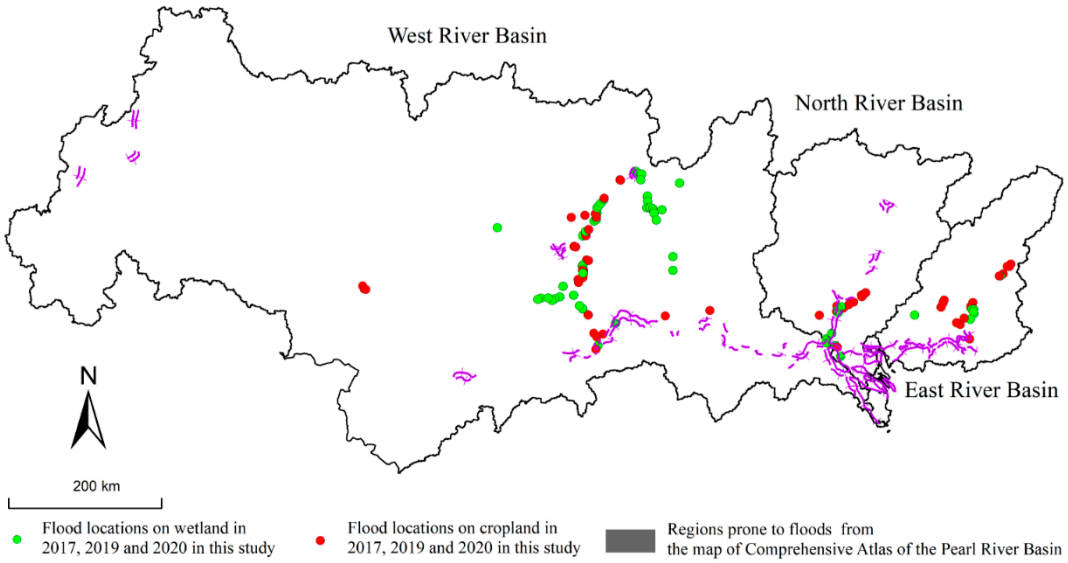

Figure 14. Comparison of the flood locations obtained in this study and the distribution of embankments obtained from the map of Comprehensive Atlas of the Pearl River Basin released by Pearl River Water Resources Commission (PRWRC) [52].

4.4. Implications for Sustainable Management of Water Resources in PRB

The interaction between climate change and anthropogenic activities will intensify the risk of floods. Zhang et al. [53] reported that annual precipitation showed an increasing trend during the period 1961–2016 under the background of global warming, which implies a flood risk in Southeast China. Li et al. [54] believed that extreme heavy precipitation events would increase flood risks during the 21st century. This study had also reported that anthropogenic activities like constructions of embankments and sand mining would affect the trend of floods. To prevent and mitigate flood hazards, we should first understand the patterns of flood hazards, for which we need to enhance flood monitoring techniques. This study comprehensively compared the flood monitoring results derived from hydrological data and Sentinel-1 images, providing a case study about the combination of Sentinel-1 images with hydrological data to monitor flood hazards in the PRB. In addition, using Sentinel-1 images to monitor floods would cost less due to its free access, wide swath and working regardless of weather conditions. With the development of cloud platforms like GEE, it is also possible to analyze the floods in large river basins or even global flood hazards using Sentinel-1 images.

Some floods in this study were not illustrated in the map of Comprehensive Atlas of the Pearl River Basin published by PRWRC, indicating that the flood control projects planned by the government would be somewhat incomplete in some regions as a large number of flood-prone areas in the upper reaches has still been ignored, and flood control measures have not been implemented. Flood control measures in the middle and lower reaches of the Pearl River have been well implemented, but more flood control measures and policies should focus on remote areas. Thus, this study's results are useful to improve the results released by the Ministry of Water Resources and could be a reference for the adjustment of flood control projects planned by the government.

Unlike most studies [20–27] which focus on urban floods, this study has highlighted that flood hazards in PRB have caused significant impacts on croplands in rural regions, which is the important agricultural product supplier and plays an important role in food safety in PRB. Figures 1 and 14 show that water conservancy facilities like embankments are currently constructed mainly in urban regions, such as the PRD. However, in the rural area in WRB, the most critical flooding region in the PRB, few embankments have been constructed. Thus, to mitigate or prevent flood hazards in a rural region and protect farm-

ers' lives and property, the government should formulate measures to strengthen the protection of cropland, such as the construction of water conservancy facilities in critical rural regions and the promotion of agriculture insurance for farmers. This study has highlighted the locations and extents of the croplands affected by flood hazards, which could be regarded as a valuable reference for the government to manage the water resources in PRB. Although flood prevention is important in rural areas, one must also recognize that ecosystems and environmental protection are equally important in such areas. Therefore, environmentally friendly flood control measures should be given priority.

5. Conclusions

This study used Sentinel-1 images to investigate floods that occurred in 2017, 2019 and 2020 in the Pearl River Basin, focusing on rural areas. The study provided a reliable flood monitoring result in PRB. The results indicated that flood locations are mainly distributed in central WRB, middle reaches of NRB and middle reaches of ERB. Collectively, the flooding patterns showed that WRB is more prone to flood hazards than NRB and ERB. In the PRB, the most vulnerable river sections to floods are Yijiang, Luoqingjiang, Qianjiang, and Xunjiang tributaries, and the lower reaches of Liujiang. In the 2017 flood, 75.0% of flood locations distributed along the major river sections, and 92.3% inundated croplands were distributed around the major river sections.

Compared with flood monitoring based on hydrological data, Sentinel-1 images have the advantage of spatial continuity. They can be an alternative in the regions with few hydrological stations. It is also recommended to combine Sentinel-1 images with hydrological data to monitor floods. This study also highlighted the severity of flood hazards in rural regions in the PRB and calls for policy overhaul to enhance flood control in the rural areas to ensure food safety. This study is a valuable reference for flood monitoring, loss assessment, and flood mitigation planning in the Pearl River Basin.

Author Contributions: Conceptualization and methodology, J.Q., P.T. and X.Y.; data collection, J.Q., B.C. and W.Z.; data analysis, J.Q., and B.C.; writing—original draft preparation, J.Q.; writing—review and editing, J.Q., E.P., P.T. and X.Y. All authors have read and agreed to the published version of the manuscript.

Funding: This research was funded by the National Natural Science Foundation of China, grant number 41871017, research support from Guangzhou University, grant number 69-18ZX1000201, Nanyang Technological University (SUG-NAP EP3/19) and the Singapore Ministry of Education (AcRF Tier1 RT6/19).

Conflicts of Interest: The authors declare no conflicts of interest.

References

1. Alexander, L.V.; Zhang, X.; Peterson, T.C.; Caesar, J.; Gleason, B.; Tank, A.; Haylock, M.; Collins, D.; Trewin, B.; Rahimzadeh, F.; et al. Global observed changes in daily climate extremes of temperature and precipitation. *J. Geophys. Res. Atmos.* **2006**, *111*, doi:10.1029/2005jd006290.
2. Qiu, J.; Yang, X.; Cao, B.; Chen, Z.; Li, Y. Effects of Urbanization on Regional Extreme-Temperature Changes in China, 1960–2016. *Sustainability* **2020**, *12*, 6560, doi:10.3390/su12166560.
3. Yang, X.; Lu, X.; Park, E.; Tarolli, P. Impacts of Climate Change on Lake Fluctuations in the Hindu Kush-Himalaya-Tibetan Plateau. *Remote Sens.* **2019**, *11*, 1082, doi:10.3390/rs11091082.
4. Lehner, B.; Doll, P.; Alcamo, J.; Henrichs, T.; Kaspar, F. Estimating the impact of global change on flood and drought risks in europe: A continental, integrated analysis. *Clim. Chang.* **2006**, *75*, 273–299, doi:10.1007/s10584-006-6338-4.
5. Huang, X.; Tan, H.; Zhou, J.; Yang, T.; Benjamin, A.; Wen, S.W.; Li, S.; Liu, A.; Li, X.; Fen, S.; et al. Flood hazard in Hunan province of China: An economic loss analysis. *Nat. Hazards* **2008**, *47*, 65–73, doi:10.1007/s11069-007-9197-z.
6. Jonkman, S.N.; Vrijling, J.K. Loss of life due to floods. *J. Flood Risk Manag.* **2008**, *1*, 43–56, doi:10.1111/j.1753-318X.2008.00006.x.
7. Sofia, G.; Roder, G.; Dalla Fontana, G.; Tarolli, P. Flood dynamics in urbanised landscapes: 100 years of climate and humans' interaction. *Sci. Rep.* **2017**, *7*, doi:10.1038/srep40527.
8. Park, E.; Huu Loc, H.; Dung Duc, T.; Yang, X.; Alcantara, E.; Merino, E.; Vu Hai, S. Dramatic decrease of flood frequency in the Mekong Delta due to river-bed mining and dyke construction. *Sci. Total Environ.* **2020**, *723*, doi:10.1016/j.scitotenv.2020.138066.

9. Yang, X.; Lu, X.; Ran, L.; Tarolli, P. Geomorphometric Assessment of the Impacts of Dam Construction on River Disconnectivity and Flow Regulation in the Yangtze Basin. *Sustainability* **2019**, *11*, doi:10.3390/su11123427.
10. Barichivich, J.; Gloor, E.; Peylin, P.; Brienen, R.J.W.; Schongart, J.; Carlo Espinoza, J.; Pattnayak, K.C. Recent intensification of Amazon flooding extremes driven by strengthened Walker circulation. *Sci. Adv.* **2018**, *4*, doi:10.1126/sciadv.aat8785.
11. Zaroug, M.A.H.; Eltahir, E.A.B.; Giorgi, F. Droughts and floods over the upper catchment of the Blue Nile and their connections to the timing of El Nino and La Nina events. *Hydrol. Earth Syst. Sci.* **2014**, *18*, 1239–1249, doi:10.5194/hess-18-1239-2014.
12. Viero, D.P.; Roder, G.; Matticchio, B.; Defina, A.; Tarolli, P. Floods, landscape modifications and population dynamics in anthropogenic coastal lowlands: The Polesine (northern Italy) case study. *Sci. Total Environ.* **2019**, *651*, 1435–1450, doi:10.1016/j.scitotenv.2018.09.121.
13. Pijl, A.; Brauer, C.C.; Sofia, G.; Teuling, A.J.; Tarolli, P. Hydrologic impacts of changing land use and climate in the Veneto lowlands of Italy. *Anthropocene* **2018**, *22*, 20–30, doi:10.1016/j.ancene.2018.04.001.
14. Zhang, Q.; Gu, X.; Vijay, P.S.; Shi, P.; Sun, P. More frequent flooding? Changes in flood frequency in the Pearl River basin, China, since 1951 and over the past 1000 years. *Hydrol. Earth Syst. Sci.* **2018**, *22*, 2637–2653.
15. Zhang, W.; Yan, Y.; Zheng, J.; Li, L.; Dong, X.; Cai, H. Temporal and spatial variability of annual extreme water level in the Pearl River Delta region, China. *Glob. Planet. Chang.* **2009**, *69*, 35–47, doi:10.1016/j.gloplacha.2009.07.003.
16. Wu, Z.; Lu, G.; Liu, Z.; Wang, J.; Xiao, H. Trends of Extreme Flood Events in the Pearl River Basin during 1951–2010. *Adv. Clim. Chang. Res.* **2013**, *4*, 110–116.
17. Zhang, Q.; Gu, X.; Singh, V.P.; Xiao, M.; Xu, C.-Y. Flood frequency under the influence of trends in the Pearl River basin, China: Changing patterns, causes and implications. *Hydrol. Process.* **2015**, *29*, 1406–1417, doi:10.1002/hyp.10278.
18. Gu, X.; Zhang, Q.; Singh, V.P.; Xiao, M.; Cheng, J. Nonstationarity-based evaluation of flood risk in the Pearl River basin: Changing patterns, causes and implications. *Hydrol. Sci. J.* **2017**, *62*, 246–258, doi:10.1080/02626667.2016.1183774.
19. Yang, T.; Xu, C.-Y.; Shao, Q.-X.; Chen, X. Regional flood frequency and spatial patterns analysis in the Pearl River Delta region using L-moments approach. *Stoch. Environ. Res. Risk Assess.* **2010**, *24*, 165–182, doi:10.1007/s00477-009-0308-0.
20. Wu, X.; Wang, Z.; Guo, S.; Liao, W.; Zeng, Z.; Chen, X. Scenario-based projections of future urban inundation within a coupled hydrodynamic model framework: A case study in Dongguan City, China. *J. Hydrol.* **2017**, *547*, 428–442, doi:10.1016/j.jhydrol.2017.02.020.
21. Du, S.; Shi, P.; Van Rompaey, A.; Wen, J. Quantifying the impact of impervious surface location on flood peak discharge in urban areas. *Nat. Hazards* **2015**, *76*, 1457–1471, doi:10.1007/s11069-014-1463-2.
22. Zhou, L.; Wu, X.; Ji, Z.; Gao, G. Characteristic analysis of rainstorm-induced catastrophe and the countermeasures of flood hazard mitigation about Shenzhen city. *Geomat. Nat. Hazards Risk* **2017**, *8*, 1886–1897, doi:10.1080/19475705.2017.1392368.
23. Zhang, W.; Cao, Y.; Zhu, Y.; Wu, Y.; Ji, X.; He, Y.; Xu, Y.; Wang, W. Flood frequency analysis for alterations of extreme maximum water levels in the Pearl River Delta. *Ocean Eng.* **2017**, *129*, 117–132, doi:10.1016/j.oceaneng.2016.11.013.
24. Zhang, H.; Ma, W.-C.; Wang, X.-R. Rapid urbanization and implications for flood risk management in hinterland of the Pearl River Delta, China: The Foshan study. *Sensors* **2008**, *8*, 2223–2239, doi:10.3390/s8042223.
25. Yang, L.; Scheffran, J.; Qin, H.; You, Q. Climate-related flood risks and urban responses in the Pearl River Delta, China. *Reg. Environ. Chang.* **2015**, *15*, 379–391, doi:10.1007/s10113-014-0651-7.
26. Zhang, Q.; Wu, Z.; Guo, G.; Zhang, H.; Tarolli, P. Explicit the urban waterlogging spatial variation and its driving factors: The stepwise cluster analysis model and hierarchical partitioning analysis approach. *Sci. Total Environ.* **2020**, 432, 432–439, doi:10.1016/j.scitotenv.2020.143041.
27. Zhang, Q.; Wu, Z.; Zhang, H.; Dalla Fontana, G.; Tarolli, P. Identifying dominant factors of waterlogging events in metropolitan coastal cities: The case study of Guangzhou, China. *J. Environ. Manag.* **2020**, *271*, doi:10.1016/j.jenvman.2020.110951.
28. Park, E. Characterizing channel-floodplain connectivity using satellite altimetry: Mechanism, hydrogeomorphic control, and sediment budget. *Remote Sens. Environ.* **2020**, *243*, doi:10.1016/j.rse.2020.111783.
29. Park, E.; Emadzadeh, A.; Alcantara, E.; Yang, X.; Ho, H.L. Inferring floodplain bathymetry using inundation frequency. *J. Environ. Manag.* **2020**, *273*, doi:10.1016/j.jenvman.2020.111138.
30. Wang, Y.; Colby, J.D.; Mulcahy, K.A. An efficient method for mapping flood extent in a coastal floodplain using Landsat TM and DEM data. *Int. J. Remote Sens.* **2002**, *23*, 3681–3696, doi:10.1080/01431160110114484.
31. Brakenridge, R.; Anderson, E. Modis-based flood detection, mapping and measurement: The potential for operational hydrological applications. In *Transboundary Floods: Reducing Risks through Flood Management*; Marsalek, J., Stancalie, G., Balint, G., Eds.; Springer: Dordrecht, The Netherlands, 2006; Volume 72, pp. 1–12.
32. Olthof, I.; Tolszczuk-Leclerc, S. Comparing Landsat and RADARSAT for Current and Historical Dynamic Flood Mapping. *Remote Sens.* **2018**, *10*, doi:10.3390/rs10050780.
33. Kuenzer, C.; Guo, H.; Huth, J.; Leinenkugel, P.; Li, X.; Dech, S. Flood Mapping and Flood Dynamics of the Mekong Delta: ENVISAT-ASAR-WSM Based Time Series Analyses. *Remote Sens.* **2013**, *5*, 687–715, doi:10.3390/rs5020687.
34. Giustarini, L.; Hostache, R.; Matgen, P.; Schumann, G.J.P.; Bates, P.D.; Mason, D.C. A Change Detection Approach to Flood Mapping in Urban Areas Using TerraSAR-X. *IEEE Trans. Geosci. Remote Sens.* **2013**, *51*, 2417–2430, doi:10.1109/tgrs.2012.2210901.
35. Goffi, A.; Stroppiana, D.; Brivio, P.A.; Bordogna, G.; Boschetti, M. Towards an automated approach to map flooded areas from Sentinel-2 MSI data and soft integration of water spectral features. *Int. J. Appl. Earth Obs. Geoinf.* **2020**, *84*, doi:10.1016/j.jag.2019.101951.

36. Li, J.; Wang, C.; Xu, L.; Wu, F.; Zhang, H.; Zhang, B. Multitemporal Water Extraction of Dongting Lake and Poyang Lake Based on an Automatic Water Extraction and Dynamic Monitoring Framework. *Remote Sens.* **2021**, *13*, 865, doi:10.3390/rs13050865.
37. Zhang, Q.; Xu, C.-Y.; Gemmer, M.; Chen, Y.D.; Liu, C. Changing properties of precipitation concentration in the Pearl River basin, China. *Stoch. Environ. Res. Risk Assess.* **2009**, *23*, 377–385, doi:10.1007/s00477-008-0225-7.
38. Zhang, Q.; Xu, C.-Y.; Zhang, Z. Observed changes of drought/wetness episodes in the Pearl River basin, China, using the standardized precipitation index and aridity index. *Theor. Appl. Climatol.* **2009**, *98*, 89–99, doi:10.1007/s00704-008-0095-4.
39. Wang, L.; Wang, K. Impacts of DEM uncertainty on estimated surface solar radiation and extracted river network. *Bull. Am. Meteorol. Soc.* **2015**, *96*, 297–304, doi:10.1175/bams-d-13-00285.1.
40. Zhang, Q.; Zhang, W.; Chen, Y.D.; Jiang, T. Flood, drought and typhoon disasters during the last half-century in the Guangdong province, China. *Nat. Hazards* **2011**, *57*, 267–278, doi:10.1007/s11069-010-9611-9.
41. Uddin, K.; Matin, M.A.; Meyer, F.J. Operational Flood Mapping Using Multi-Temporal Sentinel-1 SAR Images: A Case Study from Bangladesh. *Remote Sens.* **2019**, *11*, doi:10.3390/rs11131581.
42. Ruzza, G.; Guerriero, L.; Grelle, G.; Guadagno, F.M.; Revellino, P. Multi-Method Tracking of Monsoon Floods Using Sentinel-1 Imagery. *Water* **2019**, *11*, doi:10.3390/w11112289.
43. Gong, P.; Liu, H.; Zhang, M.; Li, C.; Wang, J.; Huang, H.; Clinton, N.; Ji, L.; Li, W.; Bai, Y.; et al. Stable classification with limited sample: Transferring a 30-m resolution sample set collected in 2015 to mapping 10-m resolution global land cover in 2017. *Sci. Bull.* **2019**, *64*, 370–373, doi:10.1016/j.scib.2019.03.002.
44. Otsu, N. A threshold selection method from gray-level histograms. *IEEE Trans. Syst. Man Cybern* **1979**, *9*, 62–66.
45. Du, Y.; Zhang, Y.; Ling, F.; Wang, Q.; Li, W.; Li, X. Water Bodies' Mapping from Sentinel-2 Imagery with Modified Normalized Difference Water Index at 10-m Spatial Resolution Produced by Sharpening the SWIR Band. *Remote Sens.* **2016**, *8*, 354, doi:10.3390/rs8040354.
46. Schlaffer, S.; Matgen, P.; Hollaus, M.; Wagner, W. Flood detection from multi-temporal SAR data using harmonic analysis and change detection. *Int. J. Appl. Earth Obs. Geoinf.* **2015**, *38*, 15–24, doi:10.1016/j.jag.2014.12.001.
47. Liang, J.; Liu, D. A local thresholding approach to flood water delineation using Sentinel-1 SAR imagery. *ISPRS J. Photogramm. Remote Sens.* **2020**, *159*, 53–62, doi:10.1016/j.isprsjprs.2019.10.017.
48. Schumann, G.J.P.; Neal, J.C.; Mason, D.C.; Bates, P.D. The accuracy of sequential aerial photography and SAR data for observing urban flood dynamics, a case study of the UK summer 2007 floods. *Remote Sens. Environ.* **2011**, *115*, 2536–2546, doi:10.1016/j.rse.2011.04.039.
49. Chung, S.Y.; Park, R.H.J.C.V.G.; Processing, I. A comparative performance study of several global thresholding techniques for segmentation. *Comput. Vis. Graph. Image Process* **1990**, *52*, 171–190.
50. Yang, X.; Lu, X. Drastic change in China's lakes and reservoirs over the past decades. *Sci. Rep.* **2014**, *4*, doi:10.1038/srep06041.
51. Lu, X.X.; Zhang, S.R.; Xie, S.P.; Ma, P.K. Rapid channel incision of the lower Pearl River (China) since the 1990s as a consequence of sediment depletion. *Hydrol. Earth Syst. Sci.* **2007**, *11*, 1897–1906, doi:10.5194/hess-11-1897-2007.
52. Pearl River Water Resources Commission. *Comprehensive Atlas of the Pearl River Basin;* Pearl River Water Resources Commission: Tianshou Road 80 Tianhe District Guangzhou China, 2012.
53. Zhang, Y.; Ren, Y.; Ren, G.; Wang, G. Precipitation Trends Over Mainland China From 1961-2016 After Removal of Measurement Biases. *J. Geophys. Res. Atmos.* **2020**, *125*, doi:10.1029/2019jd031728.
54. Li, J.; Zhang, Q.; Chen, Y.D.; Singh, V.P. Future joint probability behaviors of precipitation extremes across China: Spatiotemporal patterns and implications for flood and drought hazards. *Glob. Planet. Chang.* **2015**, *124*, 107–122, doi:10.1016/j.gloplacha.2014.11.012.